

# New Insight into the Ground State of FePc: A Diffusion Monte Carlo Study

Tom Ichibha<sup>1,\*</sup>, Zhufeng Hou<sup>2</sup>, Kenta Hongo<sup>1,2,3</sup>, and Ryo Maezono<sup>1</sup>

<sup>1</sup>School of Information Science, JAIST, Nomi, Ishikawa, Japan

<sup>2</sup>National Institute of Materials Science, Tsukuba, Ibaraki, Japan

<sup>3</sup>PRESTO, JST, Kawaguchi, Saitama, Japan

\*ichibha@icloud.com

## ABSTRACT

We have applied DMC to evaluate relative stability of the possible electronic configurations of an isolated FePc under  $D_{4h}$  symmetry, considering some fixed nodes generated from different methods. They predict  $A_{2g}$  ground state consistently, supporting preceding DFT studies, with confidence overcoming the ambiguity about exchange-correlation (XC) functionals. By comparing DMC with several XC, we clarified the importance of the short range exchange to describe the relative stability. We examined why the predicted  $A_{2g}$  is excluded from possible ground states in the recent ligand field based model. Simplified assumptions made in the superposition model are identified to give unreasonably less energy gain for  $A_{2g}$  when compared with the reality. The state is found to have possible reasons for the stabilization, reducing the occupations from an unstable anti-bonding orbital, avoiding double occupation of a spatially localized orbital, and gaining exchange energy by putting a triplet spin pair in degenerate orbitals.

## Introduction

Iron(II) Phthalocyanine (FePc) attracts recent interests for its potentials in spintronics<sup>1-3</sup> because it possesses the strong magnetic anisotropy as a molecular magnet.<sup>4</sup> It has been reported the anisotropy can be controlled by surrounding environments of molecules, such as ligands, polymorphs of molecular crystal structures *etc.*<sup>2,5,6</sup> These environments tune the electronic configuration of the central transition metal element, affecting its magnetic anisotropy. Identifying the electronic configuration under given environments is therefore the most essential starting point for further understandings and applications of the magnetic anisotropy of these compounds, stimulating intensive studies in this direction. An earlier study<sup>7</sup> reported its spin multiplicity being in between  $S = 1 \sim 2$ .<sup>7</sup> Later, Dale *et al.*<sup>8</sup> performed magnetic susceptibility measurements of  $\beta$ -FePc, reporting that the system takes  $S = 1$  in the range,  $T = 1.25 \sim 20$  K. Since then, the possible configurations within  $S = 1$  have been of the interests. Even under this constraint, no consensus has been established about its ground state configuration.

Experimentally, the most common targets are molecular crystals with lamination angles,  $\phi = 44.8^\circ$  ( $\beta$  phase/most stable structure) and  $\phi = 26.5^\circ$  ( $\alpha$  phase/quasi stable). The most stable  $\beta$  phase has been the main interest until  $\alpha$ -FePc was reported<sup>9,10</sup> to exhibit ferromagnetic transition at  $T_c = 5.6$  K, while  $\beta$  remains paramagnetic until above 1 K. The  $\alpha$  phase then attracts broader interests for its ferromagnetism with the spin anisotropy lying within its molecular plane with unquenched orbital angular momentums.<sup>2,11</sup> Under practical samples in experiments, the ground state configuration of the  $\alpha$  phase has been reported as  $E_g(a)$ , forming a consensus.<sup>1,4,11</sup>

Apart from intensive discussions on possible factors affecting the configuration in practical samples, such as inter-complex interactions in crystals<sup>6,12</sup>, the spin-orbit coupling *etc.*,<sup>2,13</sup> it is a reasonable option to start considering the simplest situation, namely, an isolated, highly symmetric molecule. Electronic structure calculations using DFT (density functional theory) have hence been made for the isolated molecule. However, even without the spin-orbit coupling, theoretical predictions have never dropped in a consensus as described below. We hence target the most simplified question, “*what is the ground state electronic configuration for the ideal isolated FePc within the non-relativistic framework?*”. Most of DFT studies so far predict  $A_{2g}$  ground state,<sup>6,14,15</sup> while a recent study<sup>15</sup> reports that the prediction actually depends on the choice of exchange-correlation (XC) functionals and Gaussian basis set level, getting both  $A_{2g}$  and  $B_{2g}$  as the possibility. The same conclusion is actually confirmed in the present study, getting mainly  $A_{2g}$ , but sometimes  $B_{2g}$  and even  $E_g(a)$  depending on XC.

Another complementary approach is the ligand field framework.<sup>2,16,17</sup> It is capable to be applied to the  $D_{4h}$  isolated molecule, predicting  $E_g(b)$  ground state for the ligand parameter choice for  $\alpha$  phase. (When the spin-orbit coupling is taken into account, it predicts a hybrid state between  $E_g(b)$  and  $B_{2g}$  as the ground state, latter of which is predicted as the first excited state when without the coupling. The magnetic anisotropy is predicted being perpendicular to [within] the molecular plane for  $E_g(b)$  [ $B_{2g}$ ]. In the hybrid state, it is within the plane despite the dominant state is  $E_g(b)$ .)<sup>2</sup> The original ligand field

model for  $D_{4h}$  requires three ligand parameters to identify the possible ground state, where  $A_{2g}$  still remains as a possibility<sup>16</sup>, not conflicting with *ab initio* DFT predictions. In a recent work<sup>17</sup>, however, the possible ground state is specified by reduced two parameters and  $A_{2g}$  has disappeared from the possibility, leading to an apparent contradiction to DFT predictions. The reduction of the freedom of parameters occurs when they employ the superposition model<sup>18</sup> under some assumptions.

The present study targets to investigate the apparent discrepancy about  $A_{2g}$  ground state between *ab initio* and ligand field model<sup>17</sup> approaches. Blocked by the ambiguity of predictions due to XC, this discrepancy has not well been addressed and investigated so far. To prevent the ambiguity, we applied (fixed-node) diffusion Monte Carlo (DMC)<sup>21</sup> to calibrate the XC dependence.<sup>3,21,22</sup> Although CASSCF (complete active space self-consistent field) seems a natural choice of trial nodes appropriate for describing the multi-reference nature in transition metals, a recent work suggests it is not necessarily the best for iron complexes, finding some DFT trial nodes are better.<sup>31</sup> Hence we tried several trial nodes generated from DFT with M06, M06L, and M06-2X functionals as well as CASSCF (Computational details in the present study are given in Supplementary Information.)

We have found all the DMC predictions support  $A_{2g}$  ground state, being consistent with most of previous DFT calculations. The apparent contradiction with the ligand field model<sup>17</sup> can be explained by further considering the validation of the assumptions in the superposition model. The assumption turns out not capable to capture the stabilizing mechanisms of  $A_{2g}$ , which are clarified by the orbital shape/occupation analysis by the present study.

## System

We investigate the ground state electronic configuration of an isolated FePc molecule under  $D_{4h}$  symmetry. While there are two preceding studies reporting the possible geometry, the one from X-ray diffraction of  $\beta$  phase<sup>23</sup> and the other from DFT geometry optimization applied to an isolated complex,<sup>23</sup> we used the latter for the present calculation (See Supplementary Information). The system accommodates six electrons in  $3d$ -shells from Fe ion. Within the constraint of spin triplet,  $S = 1$ , there are four possible configurations labeled as,

$$\begin{aligned}
 A_{2g} &: (a_g)^{\uparrow\downarrow}(e_g)^{\uparrow\uparrow}(b_{2g})^{\uparrow\downarrow} = (d_{z^2})^{\uparrow\downarrow}(d_{xz,yz})^{\uparrow\uparrow}(d_{xy})^{\uparrow\downarrow}, \\
 B_{2g} &: (a_g)^{\uparrow}(e_g)^{\uparrow\downarrow\downarrow}(b_{2g})^{\uparrow} = (d_{z^2})^{\uparrow}(d_{xz,yz})^{\uparrow\downarrow\downarrow}(d_{xy})^{\uparrow}, \\
 E_g(a) &: (a_g)^{\uparrow}(e_g)^{\uparrow\downarrow\uparrow}(b_{2g})^{\uparrow\downarrow} = (d_{z^2})^{\uparrow}(d_{xz,yz})^{\uparrow\downarrow\uparrow}(d_{xy})^{\uparrow\downarrow}, \\
 E_g(b) &: (a_g)^{\uparrow\downarrow}(e_g)^{\uparrow\downarrow\uparrow}(b_{2g})^{\uparrow} = (d_{z^2})^{\uparrow\downarrow}(d_{xz,yz})^{\uparrow\downarrow\uparrow}(d_{xy})^{\uparrow}.
 \end{aligned} \tag{1}$$

Any occupations to  $d_{x^2-y^2}$  are excluded from the possibility because the orbital makes a strong  $\sigma^*$ -coupling with neighboring ligands to get unstabilized.

## Results

### DMC results

Predictions of the relative stability among the states are shown in Fig. 1, compared with each other among DMC, CASSCF, and DFT. A pronounced feature of the present DMC predictions (shown as bold lines) is the 'N-shaped' dependence [the lowest  $A_{2g}$  and a dip at  $E_g(a)$ ]. Since CASSCF-DMC is reported to be 'not best' in the nodal quality sense<sup>31</sup>, we also performed several DFT-DMC results using M06, M06L, and M06-2X functionals for further confirmation. We see that all the DMC give the N-shape with the lowest energy by  $A_{2g}$ , being consistent with each other. For M06L, it is interesting to see that 'non-N-shape' at DFT level turns to 'N-shape' at fixed-node DMC level. Among the DFT-DMC, the M06 is found to give *variationally best* nodal surfaces, making total energies of each state lower than those by M06L and M06-2X by around  $\sim 0.4$  eV in average. We cannot make unfortunately the variational comparison between DFT-DMC and CASSCF-DMC because the latter is an all-electron simulation, while the former a pseudo potential one (See Supplementary Information for computational details).

### Inconsistency of DFT predictions

While most of preceding DFT reported  $A_{2g}$  predicted as the ground state, we clearly see here again that the prediction indeed depends on the choice of XC, as already pointed out by several authors.<sup>13,15,25</sup> Assuming the results by M06-DMC being the more reliable prediction, we can focus on its 'N-shaped' dependence being a target property to be reproduced by properly selected XC. We see that the B3LYP-DFT prediction is quite similar to the M06-DMC one, which would support the validation of DFT predictions by this functional to some extent. We could identify that the short-range exchange contribution is quite essential to reproduce the 'N-shape', as discussed below.

Looking at DFT+ $U$  results,<sup>26</sup> we see that the 'N-shape' gets recovered as  $U$  increases, corresponding to taking into account the exchange component more. The same tendency can also be confirmed by the results<sup>27</sup> using a hybrid functionals, M06.

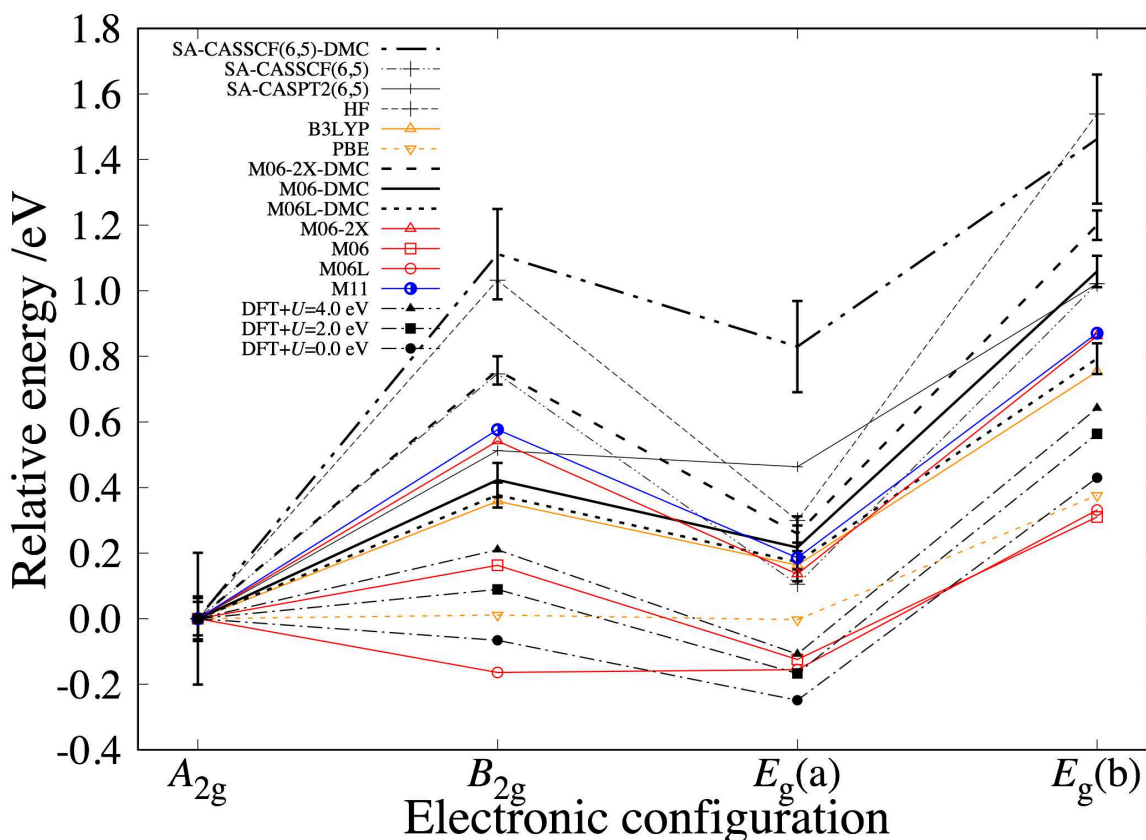


**Figure 1.** The predictions of some *ab initio* methods. This graph shows the predictions of CASSCF-DMC, DFT-DMC, HF, CASSCF, CASPT2, and some DFT calculations about the relative stability among the four electronic configurations.

In the series of M06 in Fig. 1, the Fock exchange contribution increases as M06-L(0%)  $\rightarrow$  M06(27%)  $\rightarrow$  M06-2X(54%), and it approaches to the 'N-shaped' dependence. M11 in Fig. 1 also includes the Fock exchange contribution but it is separated into short- and long-range components. The comparison between M11 and M06-2X clearly shows us which component matters: The two functionals both contain the Fock exchange at almost the same fraction in total, 54% (M06-2X) and 42.8% (M11), but they are different in their fractions of long-range component, 54% (M06-2X) and 100% (M11). Almost the same 'N-shape' for both implies that the improvement in M11 from M06-2X (taking into account the long-range exchange components) does not so matter in the present case to reproduce the 'N-shape'. Though the improvement is known to affect a lot in reproducing long-ranged natures such as van der Waals interactions,<sup>28</sup> what matters in the present case seems rather the short-range component, or to say the self-interaction nature of the exchange.

## Discussions

### Short-range exchange in DFT

The implication of the importance of the short-range exchange component is in accordance with the fact that the increase of  $U$  in DFT+ $U$  enhances the 'N-shape'. This would be encouraging to omit the costly evaluation of long-range exchange when one investigates more realistic periodic molecular crystals. Since the exchange interaction represents the energy gain by the orbital overlap only for spin-parallel pairs, it would critically affect when we estimate the energy differences between the states with different spin-pair configurations. While in DMC such factors are taken into account by default, DFT treatments require the special attention to choose XC functional so that it could include enough short-range exchange component to describe

proper trends in energy differences.

As mentioned in the introduction, it is difficult to find such experiments those are exactly realizing the isolated/non-relativistic molecular system to be compared with the present theoretical estimations. Photoelectron spectroscopy of FePc in gas phase<sup>29</sup> can be the nearest case for this purpose. Another earlier spectroscopy was reported<sup>32</sup> for the molecule in solvent, concluding  $A_{2g}$  as its ground state configuration because only this configuration can explain the observed shape of spectrum. A recent spectroscopic study<sup>29</sup> indicates B3LYP agrees reasonably well with experiment while PBE does not. This is rather consistent with our trend in Fig. 1, where PBE fails to reproduce the N-shape while B3LYP with exchange components can do it. These consistencies would support our conclusion that the N-shape by DMC describes the correct order of the energetic stability for each of the electronic configurations.

### Exchange v.s. Correlation effects

Static correlation describing multi-reference nature is captured by CASSCF beyond HF, while dynamical correlation describing hybridization between iron and ligands by CASPT2, though the second-order perturbation theory is well known to overestimate the dynamic one for open shell system<sup>30</sup>. The corresponding change in Fig. 1 can then be identified as a consequence of the correlation effect, which decreases relative energy differences among the configurations making the N-shape less pronounced. In contrast, exchange makes the shape more pronounced. We could then identify the ratio,  $\gamma = (\text{correlation/exchange})$ , would be a factor to dominate the N-shape. Ratios for M06L and PBE get larger owing to incomplete inclusion of exchange part, and then the shape would be less pronounced. A comparison between M06 and B3LYP would lead to an assumption that the shape would be dominated by the ratio rather than the absolute intensity of exchange, because their inclusion percentages of Fock exchange term are almost the same (27% and 25%) but their shapes considerably differ from each other. This might be attributed to the difference of the *ratio*  $\gamma$ .

Table 1 lists CASSCF expansion coefficients, which can be roughly considered extent of multi-reference nature. According to these values,  $A_{2g}$  has a less multi-reference nature than the others. This is just corresponding to the fact that the *amplitude* of the dependence in Fig. 1 gets reduced by CASSCF compared with HF. The reduction can be explained by the larger energy stabilizations for each configuration than in  $A_{2g}$ , those are due to the static correlations by more enhanced multi-reference nature, leading to smaller energy differences between each configuration than in HF.

**Table 1.** The multi determinants calculated by SA-CASSCF for each electronic configurations. This table shows the occupation of  $d$  shell of each determinant and its coefficient.  $\uparrow$  and  $\downarrow$  means up spin and down spin respectively. Only the dominating determinants are listed up, whose coefficient's absolute values are higher than 0.2.

state	coefficient	$3d_{xy}$	$3d_{xz}$	$3d_{yz}$	$d_{z^2}$	$d_{x^2-y^2}$
$A_{2g}$	0.985	$\uparrow\downarrow$	$\uparrow$	$\uparrow$	$\uparrow\downarrow$	
$B_{2g}$	0.924	$\uparrow\downarrow$	$\uparrow\downarrow$	$\uparrow$	$\uparrow$	
	-0.345	$\uparrow$	$\uparrow$	$\uparrow\downarrow$	$\uparrow\downarrow$	
$E_g(a)$	0.941	$\uparrow\downarrow$	$\uparrow\downarrow$	$\uparrow$	$\uparrow$	
	-0.239	$\uparrow\downarrow$	$\uparrow$	$\uparrow$	$\uparrow$	$\downarrow$
$E_g(a)$	0.778	$\uparrow$	$\uparrow\downarrow$	$\uparrow$	$\uparrow\downarrow$	
	-0.382	$\uparrow$	$\uparrow\downarrow$	$\uparrow$	$\uparrow$	$\downarrow$

Though we cannot make clear statements on how the ratio  $\gamma$  in XC affects the qualities of nodal surfaces in FN-DMC, but we can see that the *amplitude* of the dependence in Fig. 1 gets larger in the order as M06L  $\rightarrow$  M06 (variationally best among DFT-DMC)  $\rightarrow$  M06-2X getting closer to CASSCF-DMC. This trend can be regarded to be driven by the decrease of  $\gamma$  for the nodal surface generation by DFT. The *location* of CASSCF-DMC at the end of this trend would be consistent with the preceding report<sup>31</sup> in the sense that the incomplete inclusion of (short-range) correlations in CASSCF leads to the diminished  $\gamma$  for nodal surface generation.

### Comparison with superposition model

The present DMC again supports the preceding DFT predictions of  ${}^3A_{2g}$  ground state. Such a possibility is, however, not permitted by the recent 'ligand field'-based model,<sup>17</sup> as shown in Fig. 3 in their paper. We can explain this apparent contradiction by examining the assumptions made in the models. Key is the reduction of number of ligand parameters to specify the ground state in the model. Original ligand field model for  $D_{4h}$  requires three parameters, ( $D_q, D_s, D_t$ ), to specify it, as in the studies,<sup>2,16</sup> where  ${}^3A_{2g}$  is still in the possibility for the ground state (e.g. in Fig. 2 in the paper by Miedema *et al.*<sup>16</sup>). In the

recent study by Kuz'min *et al.*,<sup>17</sup> however, the ground state is specified only by two ligand parameters under the constraint,  $D_t = (2/35) \cdot 10D_q$ , denying the  ${}^3A_{2g}$  possibility. The constraint comes from the more restricted geometry than  $D_{4h}$  under the assumptions by the superposition model.<sup>18</sup> It assumes that (a) only the nearest neighboring ligands (N in this case) are considered, (b) ligand fields are specified only via bond-length dependence, (c) Total ligand field is a superposition of each ligand contribution, (d) Each contribution is assumed being axially symmetric around the intervening bond between the ligand and central element (Fe-N in this case). The assumption makes the system perfect square being able to put a Fe-N bond as  $x$  (or  $y$ ) axis to get more constraint, as explained in Kuz'min *et al.*<sup>17</sup> We thus notice that the  ${}^3A_{2g}$  possibility has disappeared by this assumption.

The assumption, especially (d), seems to be easily refuted by the *ab initio* analysis for realistic treatments of actual ligands. The left panel in Fig. 2 shows the shape of  $e_g$  evaluated by SA-CASSCF(6,5), being obviously not the case of the assumption (d). We can give further possible explanations why the model assumption makes the  ${}^3A_{2g}$  unstabilized more than the *ab initio* prediction: From the occupations given in Eq. (1), we notice that  ${}^3A_{2g}$  is stabilized by reducing the number of the  $e_g$  occupation. As seen in the left panel (Fig. 2), the orbital forms strong  $\pi$ -coupling with neighboring N, spreading along the molecular plane. The orbital has the opposite phase to that of Fe, forming an unstabilized anti-bonding state. The  ${}^3A_{2g}$  stabilizes itself by reducing such an energy loss made by the  $e_g$  occupation. This stabilization mechanism cannot be captured by the assumptions of superposition model at all. Another mechanism would be captured by the right panel of Fig. 2, where  $b_{2g}$  orbital stabilizes itself by leaking its distribution toward outer ligands, which is not taken into account in the model. The model then describes the spurious confinement for the electrons in  $b_{2g}$  orbital, getting its energy level increased than the *ab initio* estimation. This would also underestimate the stabilization of  ${}^3A_{2g}$  via  $b_{2g}$  occupation, and hence the state has disappeared from the possibility of the most stable state.

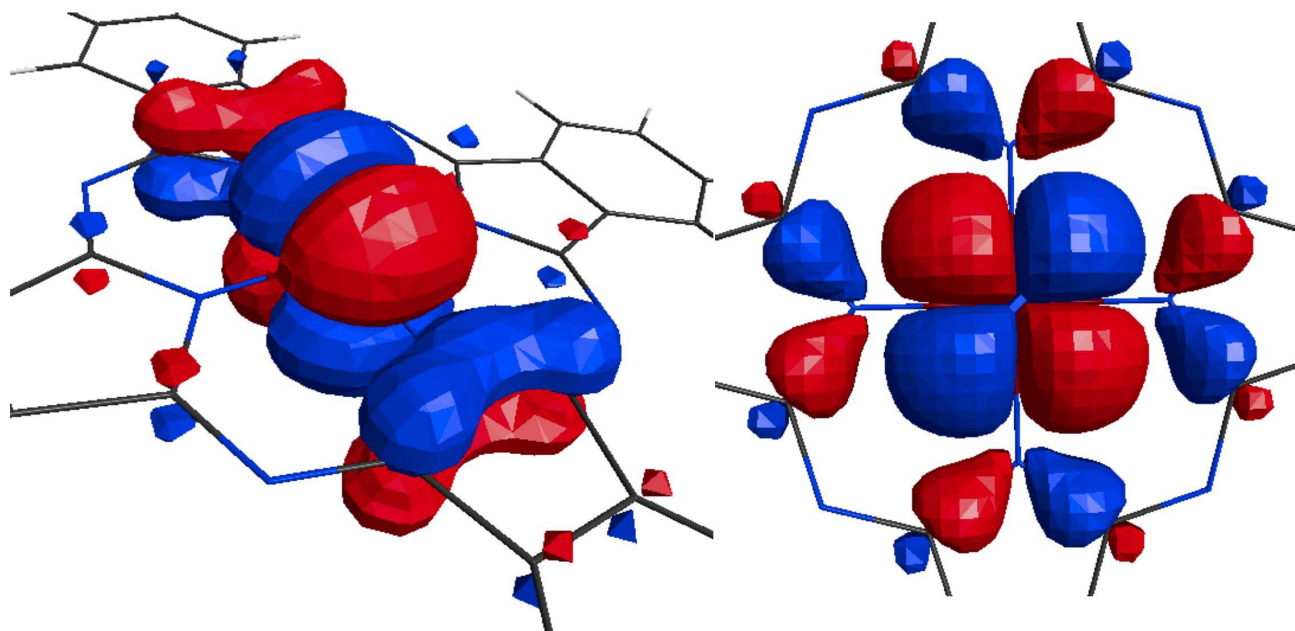


**Figure 2.** The figures of 3d orbitals.  $e_g$  (left) and  $b_{2g}$  (right) orbitals are evaluated by SA-CASSCF(6,5).

As a further possible explanation for the stabilization of  $A_{2g}$  as well as that of  $E_g(a)$ , we could take the energy loss due to the double occupancy on the spatially localized orbitals. Counting the double occupancies of  $a_g/e_g/b_{2g}$  orbitals in each state, it is 1/0/1 [ $A_{2g}$ ], 0/2/0 [ $B_{2g}$ ], 0/1/1 [ $E_g(a)$ ], and 1/1/0 [ $E_g(b)$ ], corresponding to a problem how to assign two double occupancies to each orbital. When the  $U$  is introduced, the system wants to avoid the double occupancy in a localized orbital, and then prefers to put it on  $b_{2g}$  with more spreading  $d_{xy}$ . The states having a  $d_{xy}$  double occupancy then stabilized relatively to get 'N-shaped' dependence in Fig. 1. The further stabilization of  $A_{2g}$  over  $E_g(a)$  would be explained when we look at a triplet spin pair assigned in which orbital. In  $A_{2g}$ , the pair is between  $d_{zx}$  and  $d_{yz}$  which are degenerated, while in  $E_g(a)$  they are between  $d_{z^2}$  and one of the  $d_{zx,yz}$ . The exchange energy gain is expected to be larger when the pair is within the degenerated orbitals, making a possible explanation for the stabilization.



## Conclusion

To conclude, we have applied DMC with the SA-CASSCF and DFT (M06, M06L and M06-2X) nodes to evaluate relative stability of the possible electronic configurations of an isolated FePc under  $D_{4h}$  symmetry. All the DMC simulations predict the ground state to be  $A_{2g}$ , supporting several preceding DFT results,<sup>6,14,15</sup> though they have been regarded not well convincing because of the ambiguity about XC, as some DFT results predict different configuration.<sup>13,15,25</sup> By making comparisons between DMC and several XC, we clarified the importance of the short range exchange effect to reproduce proper relative stability among the states. We found M06 gives the variationally best fixed node for DMC. Interestingly, within the DFT framework, the B3LYP-DFT prediction was closest to the M06-DMC one. Getting confidence about the prediction, we examined why the predicted  $A_{2g}$  is excluded from possible ground states in the recent ligand field based model.<sup>17</sup> The assumptions to simplify the model are identified to give unreasonably less energy gain for  $A_{2g}$  when compared with the reality. The state is found to have possible reasons for the stabilization, reducing the occupations from an unstable anti-bonding orbital, preventing double occupancies in a spatially localized orbital, and gaining exchange energy by putting a triplet spin pair into degenerated orbitals.

FePc is a typical molecule of  $MN_4$  macrocycles ( $M$  = transition metal), which show a promising electrochemical catalytic activity for the reduction of molecular oxygen. The binding of molecular oxygen to the  $MN_4$  catalyst involves binding to the  $d$ -orbitals of the central metal in the macrocyclic structure and will be influenced by the electronic density located on those orbitals.<sup>33</sup> To the best of our knowledge, this is the first work which takes into account the many-body wavefunctions to determine unambiguously the ground state of  $3d$ -orbitals in FePc molecule. We believe that our results would provide useful hints about understanding the interaction of  $O_2$  molecules with active sites in FePc-based catalysts. As mentioned above, the short range exchange interaction is very important to describe the relative stability of different states of FePc molecule. This provides an important insight into the choice of XC in *ab initio* molecular dynamics studies<sup>34</sup> on oxygen reduction mechanism in  $FeN_4$  macrocycles.

## References

1. Kroll, T. *et al.* Transition metal phthalocyanines: Insight into the electronic structure from soft x-ray spectroscopy. *J. Chem. Phys.* **137**, 054306; 10.1063/1.4738754 (2012).
2. Fernández-Rodríguez, J., Toby, B. & van Veenendaal, M. Mixed configuration ground state in iron(II) phthalocyanine. *Phys. Rev. B* **91**, 214427–214433; 10.1103/PhysRevB.91.214427 (2015).
3. de la Torre, G., Bottari, G., Hahn, U. & Torres, T. Functional Phthalocyanine Molecular Materials (ed. Jiang, J.) 1–44 (Springer Verlag Heidelberg, 2010).
4. Filoti, G., Kuz'min, M. D. & Bartolomé, J. Mössbauer study of the hyperfine interactions and spin dynamics in  $\alpha$ -iron(I) phthalocyanine. *Phys. Rev. B* **74**, 134420–134432; 10.1103/PhysRevB.74.134420 (2006).
5. Tsukahara, N. *et al.* Adsorption-Induced Switching of Magnetic Anisotropy in a Single Iron(II) Phthalocyanine Molecule on an Oxidized Cu(110) Surface. *Phys. Rev. Lett.* **102**, 167203; 10.1103/PhysRevLett.102.167203 (2009).
6. Nakamura, K. *et al.* Constraint density functional calculations for multiplets in a ligand-field applied to Fe-phthalocyanine. *Phys. Rev. B* **85**, 235129; 10.1103/PhysRevB.85.235129 (2012).
7. Klemm, L. & Klemm, W. Magnetochemische Untersuchungen, XIV. Das magnetische Verhalten einiger Schwermetallverbindungen des Phthalocyanins. *J. Prakt. Chem.* **143**, 82; 10.1002/prac.19351430108 (1935).
8. Dale, B. W., Williams, R. J. P., Johnson, C. E. & Thorp, T. L.  $S = 1$  Spin State of Divalent Iron. I. Magnetic Properties of Phthalocyanine Iron (II). *J. Chem. Phys.* **49**, 3441; 10.1063/1.1670617 (1968).
9. Sellers, S. P., Korte, B. J., Fitzgerald, J. P., Reiff, W. M. & Yee, G. T. Canted Ferromagnetism and Other Magnetic Phenomena in Square-Planar, Neutral Manganese(II) and Iron(II) Octaethyltetraazaporphyrins. *J. Am. Chem. Soc.* **120**, 4662; 10.1021/ja973787a (1998).
10. Yee, G. T., Korte, B. J., Sellers, S. P., Reiff, W. M. & Frommen, C. M. An Internal Hyperfine Field of 62.4 T in Ferromagnetically Ordered  $\alpha$ -Iron(II) Octaethyl-Tetraazaporphyrin. *Mol. Cryst. Liq. Cryst. Sci. Technol.* **335**, 23; 10.1080/10587259908028848 (1999).
11. Bartolomé, J. *et al.* Highly unquenched orbital moment in textured Fe-phthalocyanine thin films. *Phys. Rev. B* **81**, 195405–195412; 10.1103/PhysRevB.81.195405 (2010).
12. Bidermane, I. *et al.* Characterization of gas phase iron phthalocyanine with X-ray photoelectron and absorption spectroscopies. *physica status solidi (b)* **252**, 1259–1265; 10.1002/pssb.201451147 (2015).

13. Reynolds, P. A. & Figgis, B. N. Metal Phthalocyanine Ground States: Covalence and ab Initio Calculation of Spin and Charge Densities. *Inorg. Chem.* **30**, 2294–2300; 10.1021/ic00010a015 (1991).
14. Liao, M.-S. & Scheiner, S. Electronic structure and bonding in metal phthalocyanines, Metal=Fe, Co, Ni, Cu, Zn, Mg. *J. Chem. Phys.* **114**, 9780; 10.1063/1.1367374 (2001).
15. Marom, N. & Kronik, L. Density functional theory of transition metal phthalocyanines, II: electronic structure of MnPc and FePc-symmetry and symmetry breaking. *Appl. Phys.* **95**, 165–172; 10.1007/s00339-008-5005-1 (2009).
16. Miedema, P. S., Stepanow, S., Gambardella, P. & de Groot, F. M. F. 2p x-ray absorption of iron-phthalocyanine. *J. Phys.: Conf. Ser.* **190**, 012143–012148; 10.1088/1742-6596/190/1/012143 (2009).
17. Kuz'min, M. D., Savoyant, A. & Hayn, R. Ligand field parameters and the ground state of Fe(II) phthalocyanine. *J. Chem. Phys.* **138**, 244308–244317; 10.1063/1.4811110 (2013).
18. Newman, D. J. & Ng, B. The superposition model of crystal fields. *Rep. Prog. Phys.* **52**, 699; 10.1088/0034-4885/52/6/002 (1989).
19. Foulkes, W. M. C., Mitas, L., Needs, R. J. & Rajagopal, G. Quantum Monte Carlo simulations of solids. *Rev. Mod. Phys.* **73**, 33; 10.1103/RevModPhys.73.33 (2001).
20. Hongo, K. & Maezono, R. A benchmark quantum Monte Carlo study of the ground state chromium dimer. *Int. J. Quant. Chem.* **112**, 1243–1255; 10.1002/qua.23113 (2012).
21. Hongo, K., Watson, M. A., Iitaka, T., Aspuru-Guzik, A. & Maezono, R. Diffusion Monte Carlo Study of Para-Diiodobenzene Polymorphism Revisited. *J. Chem. Theory Comput.* **11**, 907–917; 10.1021/ct500401p (2015).
22. Hongo, K., Cuong, N. T. & Maezono, R. The Importance of Electron Correlation on Stacking Interaction of Adenine-Thymine Base-Pair Step in B-DNA: A Quantum Monte Carlo Study. *J. Chem. Theory Comput.* **9**, 1081–1086; 10.1021/ct301065f (2013).
23. Kirner, J. F., Dow, W. & Scheidt, W. R. Molecular Stereochemistry of Two Intermediate-Spin Complexes. Iron(II) Phthalocyanine and Manganese(II) Phthalocyanine. *Inorg. Chem.* **15**, 1685–1690; 10.1021/ic50161a042 (1976).
24. Sumimoto, M., Kawashima, Y., Hori, K. & Fujimoto, H. Theoretical investigation of the molecular and electronic structures and excitation spectra of iron phthalocyanine and its derivatives, FePc and FePcL<sub>n</sub> (L=Py, CN<sup>-</sup>; n=1,2). *Dalton Trans.* 5737–5746; 10.1039/B823309H (2009).
25. Kuz'min, M. D., Hayn, R. & Oison, V. Ab initio calculated XANES and XMCD spectra of Fe(II) phthalocyanine. *Phys. Rev. B* **79**, 024413; 10.1103/PhysRevB.79.024413 (2009).
26. Himmetoglu, B., Floris, A., de Gironcoli, S. & Cococcioni, M. Hubbard-Corrected DFT Energy Functionals: The LDA+U Description of Correlated Systems. *Int. J. Quant. Chem.* **114**, 14–39; 10.1002/qua.24521 (2014).
27. Peverati, R. & Truhlar, D.G. Quest for a universal density functional: the accuracy of density functionals across a broad spectrum of databases in chemistry and physics. *Phil. Trans. R. Soc. A* **372**; 10.1098/rsta.2012.0476 (2014).
28. Tsuneda, T. & Hirao, K. Long-range correction for density functional theory. *Wiley Interdiscip. Rev. Comput. Mol. Sci.* **4**, 375–390; 10.1002/wcms.1178 (2014).
29. Brena, B. *et al.* Valence-band electronic structure of iron phthalocyanine: An experimental and theoretical photoelectron spectroscopy study. *J. Chem. Phys.* **134**, 074312; 10.1063/1.3554212 (2011).
30. Ghigo, G. *et al.* A modified definition of the zeroth-order Hamiltonian in multiconfigurational perturbation theory (CASPT2). *Chem. Phys. Lett.* **396**, 142; 10.1016/j.cplett.2004.08.032 (2004).
31. Fumanal, M. *et al.* Diffusion Monte Carlo Perspective on the Spin-State Energetics of [Fc(NCH)<sub>6</sub>]<sup>2+</sup>. *J. Chem. Theory Comput.* **12**, 4233; 10.1021/acs.jctc.6b00332 (2016).
32. M.J. Stillman & A.J. Thomson Assignment of the charge-transfer bands in some metal phthalocyanines. Evidence for the S = 1 state of iron (II) phthalocyanine in solution. *J. Chem. Soc., Faraday Trans. 2* **70**, 790–804; 10.1039/F29747000790 (1974).
33. Zagal, J.H., Páez, M. A. & Silva, J.F. N<sub>4</sub>-Macrocyclic Metal Complexes (ed. Zagal, J.H.) 41-82 (Springer New York, 2006).
34. Car, R. & Parrinello, M. Unified Approach for Molecular Dynamics and Density-Functional Theory. *Phys. Rev. Lett.* **55**, 2471–2474; 10.1103/PhysRevLett.55.2471 (1985).

## Acknowledgments

We are grateful to Prof. Kiyo Terakura for leading us to this challenging topic, to Dr. Yukio Kawashima for his advice on the generation of CASSCF wavefunctions, and to Prof. E.D. Jemmis for his enlightening comments. We also thank the Computational Materials Science Initiative (CMSI/Japan) for the computational resources, SR16000 (Center for Computational Materials Science of the Institute for Materials Research, Tohoku University/Japan) and K-computer (Riken/Japan). The computation in this work has been partially performing using the facilities of the Center for Information Science in JAIST. K.H. is grateful for financial support from a KAKENHI grant (15K21023), a Grant-in-Aid for Scientific Research on Innovative Areas (16H06439), PRESTO and the Materials research by Information Integration Initiative (MI<sup>2</sup>I) project of the Support Program for Starting Up Innovation Hub from Japan Science and Technology Agency (JST). R.M. is grateful for financial support from MEXT-KAKENHI grants 26287063 and that from the Asahi glass Foundation.

## Author contributions

T.I. initiated and performed main calculations under the supervision by K.H. and R.M., and Z.H. performed DFT+*U* calculations. Data is analyzed by all the authors. All the authors contributed the paper, section by section, finally organized to a manuscript.

## Additional information

Competing financial interests: The authors declare no competing financial interests.



## Supplementary Information

### SA-CASSCF calculation

We performed CASSCF calculations using GAMESS (ver. 5DEC2014R1)<sup>1,2</sup> to generate the multi-determinant wave functions. There have been several DMC studies applied to the systems including transition metal elements with the fixed nodes generated by HF or post HF methods.<sup>3,4</sup> Evaluations of energy differences by DMC include the study by ROHF-DMC<sup>5</sup>, estimating the difference between the first and second excited states of free base porphyrin, getting deviations within 0.1 eV from experimental values. Dubecky *et al.*<sup>6</sup> evaluated the first excitation energies of cis- (trans-) azobenzene using CASSCF-DMC, getting the deviation within 0.3 (0.01) eV. Zimmerman *et al.*<sup>7</sup> applied it to methylene to get deviations within 0.3 eV for differences between electronic configurations regardless of the active space sizes.

There are two options of CASSCF, state-specific CASSCF (SS-CASSCF) and state-averaged CASSCF (SA-CASSCF). In SA-CASSCF, common orbitals are applied to all the states to be evaluated while SS-CASSCF uses different ones optimized for each state individually. For the purpose to evaluate energy differences used as CASSCF-DMC, SA-CASSCF is known to be appropriate choice.<sup>8,9</sup> For excitation energies of an acrolein molecule, SS-CASSCF and SA-CASSCF trial nodes are compared in DMC to get the conclusion that only SA-CASSCF gives reasonable estimations,<sup>8,9</sup> probably due to the better error cancellations. Based on that, we generated trial nodes by SA-CASSCF.

All the elements are described as 'all-electron', getting the total number of electrons being 290. The molecular orbitals are expanded by 6-31G\*\* Gaussian basis sets. As a nature of SA-CASSCF, we had to use the same geometries commonly for all the states. The justifying discussions are given later. The size of active space is taken as CAS(6,5) because it is almost the tractable limit within the available computational resources, especially for SA-CASSCF. We also performed SA-CASPT2 with the same conditions.

### DFT calculations

We performed DFT calculations using Gaussian09<sup>10</sup>. We run all-electron calculations with def2QZVP basis set to compare DFT results. We used Burkatzki pseudo potentials with triple- $\zeta$  valence basis set to generate the trial nodes for DMC.<sup>11</sup>

To get a symmetry-adapted state for each electronic configuration in a DFT simulation, we used "guess=alter" and "scf=symm" implemented in Gaussian09: We first give an initial guess appropriate for the target state by "guess=alter", and then fix the symmetries of the all occupied orbitals during its SCF procedure by "scf=symm".

### DFT+U calculations

We have performed the DFT+U calculations for FePc molecule by using a simplified version of Cococcioni and de Gironcoli<sup>12</sup>, as implemented in QUANTUM ESPRESSO package<sup>13</sup>. Several different values (0, 2 and 4 eV) have been considered for Hubbard  $U$  parameter for Fe  $3d$  orbitals. We have employed ultrasoft pseudopotentials generated with the Rappe-Rabe-Kaxiras-Joannopoulos recipe<sup>14</sup> to represent electron-ion interaction. The electronic exchange-correlation potential was calculated within the generalized gradient approximation (GGA) using the scheme of Perdew-Burke-Ernzerhof (PBE)<sup>15</sup> and the spin-polarization was taken into account. The electronic wave functions were expanded in plane waves with an energy cutoff of 35 Ry while for the charge density the energy cutoff was taken to 350 Ry. The isolated FePc molecule was simulated in a simple tetragonal cell of  $27 \times 27 \times 12 \text{ \AA}^3$ . Brillouin-zone integrations were approximated using a  $\Gamma$  point. The atomic positions of FePc molecule were optimized till the residual forces were less than 0.01 eV/ $\text{\AA}$ .

### Jastrow factor

We adopted a Jastrow factor<sup>16</sup> multiplied by determinant(s) to form a guiding function for DMC, imposing Kato's cusp conditions.<sup>17</sup> We used a function form implemented in CASINO<sup>18</sup> including electron-electron ( $u$ ), electron-nuclei ( $\chi$ ), and electron-electron-nuclei ( $f$ ) terms. Considering spin polarizations,  $u$  and  $\chi$  ( $f$ ) terms are expanded upto 8th (2nd) order of the power of inter-particle distances, getting total 144 variational parameters. Cutoff lengths for these terms are fixed as the recommended values by the implementation, and all the linear variational parameters are optimized by 'varmin-linjas' scheme.<sup>19</sup> For all-electron DMC, we also used the cusp-correction scheme<sup>20</sup> for possible electron-nuclei coalescence. All the present QMC simulations were done using CASINO (ver. 2.13)<sup>18</sup>.

### Extrapolation of time step error

For time-step error corrections in DMC,<sup>21</sup> we used an extrapolation scheme<sup>22</sup> using two time steps,  $\tau_1 = \tau_{max}$  and  $\tau_2 = \tau_{max}/4$ .  $\tau_{max}$  is taken so that it is the largest possible below which the error is proportional to  $\tau$ . From the results,  $E_j \pm \sigma_j$  by  $\tau_j$  ( $j = 1, 2$ ), the extrapolation is evaluated as,  $E(\tau \rightarrow 0) = (\tau_2 E_1 - \tau_1 E_2) / (\tau_2 - \tau_1)$  and  $E(\tau \rightarrow 0) = (\tau_2 E_1 - \tau_1 E_2) / (\tau_2 - \tau_1)$  and  $\sigma(\tau \rightarrow 0) = (\sigma_1^2 \tau_2^2 + \sigma_2^2 \tau_1^2) / (\tau_2 - \tau_1)^2$ .

For all electron calculations, It is proposed<sup>22</sup> to take  $\tau_{max} < 1/(3Z^2)$  where  $Z$  is the maximum atomic number within the system. Using  $Z = 26$  for the present case, we chose  $\tau_{max} = 4.0 \times 10^{-4} a.u.$  for SA-CASSCF-DMC. The choice actually proved

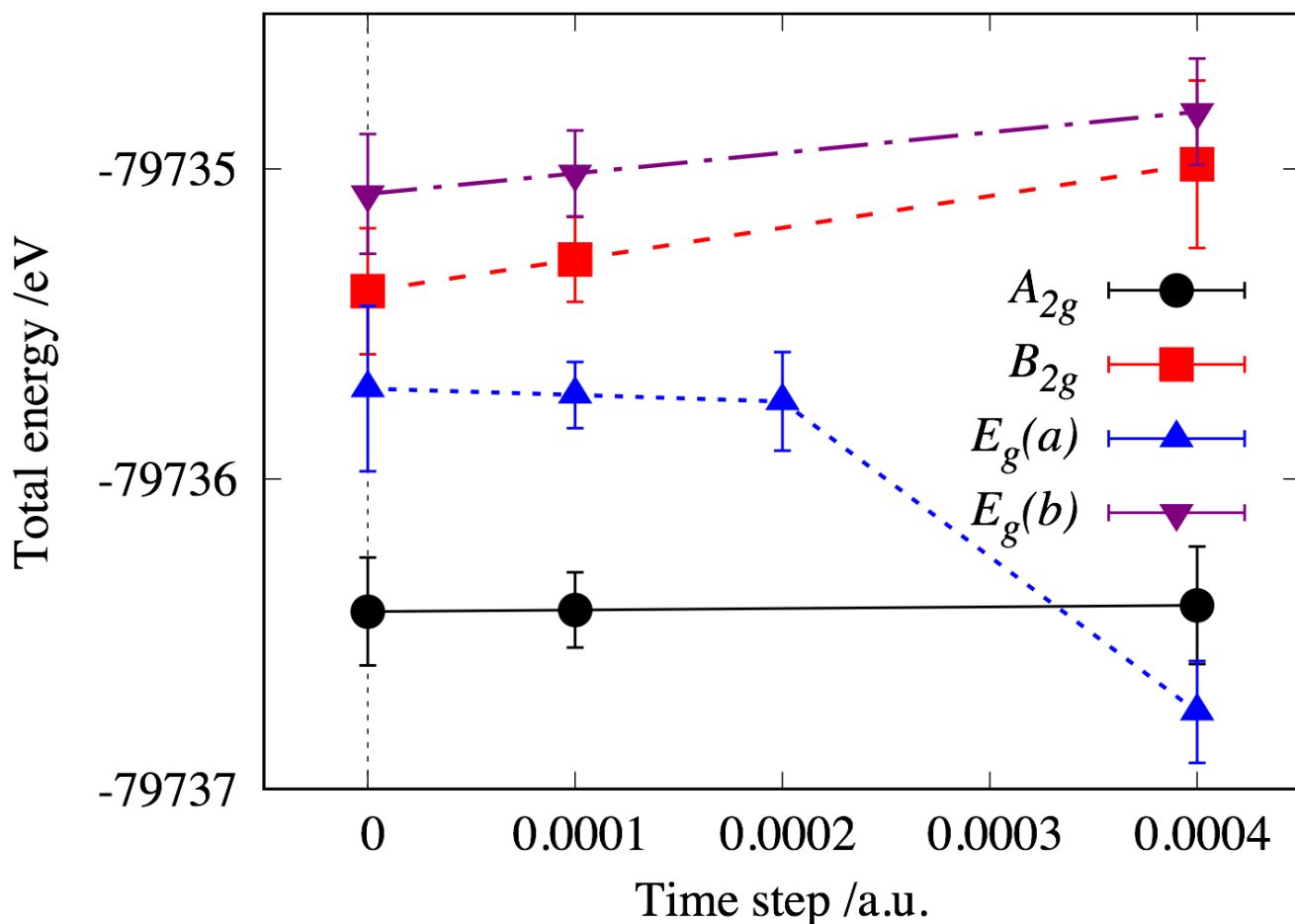


**Figure 3.** The extrapolation of DMC results. We can identify the ground state as  $A_{2g}$  with  $1\sigma$  statistical confidence, while we cannot for other excited states. Except  $E_g(a)$ , linear extrapolations below  $\tau_{\max} = 0.0004$  works well. For  $E_g(a)$ , we extrapolate using  $\tau_{\max} = 0.0002$ , instead.

to work except  $E_g(a)$  as discussed later. The best practice is known<sup>22</sup> to accumulate eight times larger steps for  $\tau_2$  than that for  $\tau_1$  to minimize computational costs.

For pseudo potential calculations,  $\tau_1 = 4.0 \times 10^{-3}$  and  $\tau_2 = 1.0 \times 10^{-3}$  were chosen for DFT-DMC. These values are larger than those of SA-CASSCF-DMC. A necessary resolution in time step is larger in the pseudo potential case than in the all-electron because random walkers diffuse on shallower potentials.

### Effects of geometry differences

As mentioned above, SA-CASSCF-DMC restricts us to use the same geometry<sup>23</sup> to all the states of electronic configurations. When the optimized geometry for each state largely differs from each other, this restriction could make the estimation poor. SA-CASSCF-DMC for an acrolein molecule<sup>8</sup> seems to be the case that it gave the overestimation of the excitation energy by  $\sim 150$  meV: Though it is not explicitly stated in their paper,<sup>8</sup> the bond length between carbon and oxygen gets elongated by 8 %<sup>24,25</sup> when the system is excited. Because of the restriction, however, SA-CASSCF-DMC cannot take into account the relaxation energy gain by the elongation, and this is quite likely to be an origin of the overestimation. To examine if this matters in the present case, we evaluated the energy gains by the relaxation from the geometry used in SA-CASSCF, as tabulated in Tab. 2. It is confirmed that the gains remain within 1.3 %, corresponding to 7.7 meV which is negligibly small compared to the statistical errors and to the energy scale in Fig. 1 in the paper. The largest relaxation is found to occur on the bond between iron and neighboring nitrogen, which is confirmed to be within 0.26 % at most. The geometry insensitivity to the occupations to be considered is, incidentally, in accordance with a report<sup>26</sup> that the Fe-N bonding length is mainly dominated by the occupation number of  $d_{x^2-y^2}$ , which is not considered here, though the conclusion is drawn from Fe porphyrin case. The insensitivity could justify the use of the same geometry to evaluate the relative stabilities among the states.

**Table 2.** The energy gains and the bond length owing to geometry optimization. B3LYP-DFT estimations of geometry relaxation gains,  $\Delta E$ , and changes in the Fe-N bond lengths ( $R_{\text{Fe-N}}$ ).  $\Delta E$  is defined as the gain when the geometries are optimized from the common structure<sup>23</sup> used in the present SA-CASSCF. For each  $E_g$  state, two bond lengths are given because it falls into  $D_{2h}$  from  $D_{4h}$  by the relaxation.

state	$\Delta E_g$ (meV)	$R_{\text{Fe-N}}$ (Å)
$A_{2g}$	-0.0	1.949
$B_{2g}$	-4.7 (-1.3 %)	1.946
$E_g(a)$	-1.1 (-1.2 %)	1.946/1.950
$E_g(b)$	-7.7 (-1.0 %)	1.941/1.951

## References

- Schmidt, M. W. *et al.* General atomic and molecular electronic structure system. *J. Comput. Chem.* **14**, 1347–1363; 10.1002/jcc.540141112 (1993).
- Gordon, M.S. & Schmidt, M.W. Theory and Applications of Computational Chemistry (ed. Dykstra C.E. *et al.*) 1167–1189 (Elsevier, 2005).
- Hongo, K. & Maezono, R. A benchmark quantum Monte Carlo study of the ground state chromium dimer. *Int. J. Quant. Chem.* **112**, 1243–1255; 10.1002/qua.23113 (2012).
- Koseki, J., Maezono, R., Tachikawa, M., Towler, M. D. & Needs, R. J. Quantum Monte Carlo study of porphyrin transition metal complexes. *J. Chem. Phys.* **129**, 085103; 10.1063/1.2966003 (2008).
- Aspuru-Guzik, A., Akramine, O. E., Grossman, J. C. & Lester, W. A. Quantum Monte Carlo for electronic excitations of free-base porphyrin. *J. Chem. Phys.* **120**, 3049–3050; 10.1063/1.1646356 (2004).
- Dubecký, M., Derian, R., Mitas, L. & Štich, I. Ground and excited electronic states of azobenzene: A quantum monte carlo study. *J. Chem. Phys.* **133**, 244301; 10.1063/1.3506028 (2010).
- Zimmerman, P. M., Toulouse, J., Zhang, Z., Musgrave, C. B. & Umrigar, C. J. Excited states of methylene from quantum monte carlo. *J. Chem. Phys.* **131**, 124103; 10.1063/1.3220671 (2009).
- Bouabça, T., Ben Amor, N., Maynau, D. & Caffarel, M. A study of the fixed-node error in quantum Monte Carlo calculations of electronic transitions: The case of the singlet  $n \rightarrow \pi^*$  (CO) transition of the acrolein. *J. Chem. Phys.* **130**, 114107; 10.1063/1.3086023 (2009).
- Toulouse, J., Caffarel, M., Reinhardt, P., Hoggan, P. E. & Umrigar, C. J. Advances in the Theory of Quantum Systems in Chemistry and Physics (ed. Hoggan, E.P. *et al.*) 343–351 (Springer Netherlands, 2012).
- Frisch, M.J. *et al.*, Gaussian 09 Revision D.01. Gaussian Inc. Wallingford CT 2009.
- Burkatzki, M., Filippi, C. Dolg, M.J. Energy-consistent pseudopotentials for quantum Monte Carlo calculations. *J. Chem. Phys.* **126**, 234105; 10.1063/1.2741534 (2007).
- Cococcioni, M. & de Gironcoli, S. Linear response approach to the calculation of the effective interaction parameters in the LDA + U method. *Phys. Rev. B* **71**, 035105; 10.1103/PhysRevB.71.035105 (2005).
- Giannozzi, P. *et al.* QUANTUM ESPRESSO: a modular and open-source software project for quantum simulations of materials. *J. Phys.: Condens. Mat.* **21**, 395502; 10.1088/0953-8984/21/39/395502 (2009).
- Rappe, A.M., Rabe, K.M., Kaxiras, E. & Joannopoulos, J.D. Optimized Pseudopotentials. *Phys. Rev. B* **41**, 1227; 10.1103/PhysRevB.41.1227 (1990).
- Perdew, J.P., Burke, K. & Ernzerhof, M. Generalized Gradient Approximation Made Simple. *Phys. Rev. Lett.* **77**, 3865; 10.1103/PhysRevLett.77.3865 (1996).
- Drummond, N. D., Towler, M. D. & Needs, R. J. Jastrow correlation factor for atoms, molecules, and solids. *Phys. Rev. B* **70**, 235119; 10.1103/PhysRevB.70.235119 (2004).
- Kato, T. On the eigenfunctions of many-particle systems in quantum mechanics. *Communications on Pure and Applied Mathematics* **10**, 151–177; 10.1002/cpa.3160100201 (1957).

18. Needs, R., Towler, M., Drummond, N. & Ríos, P. L. Continuum variational and diffusion quantum Monte Carlo calculations. *J. Phys. Condens. Matter* **22**, 023201; 10.1088/0953-8984/22/2/023201 (2010).
19. Drummond, N. D. & Needs, R. J. Variance-minimization scheme for optimizing Jastrow factors. *Phys. Rev. B* **72**, 085124; 10.1103/PhysRevB.72.085124 (2005).
20. Ma, A., Towler, M. D., Drummond, N. D. & Needs, R. J. Scheme for adding electron-nucleus cusps to Gaussian orbitals. *J. Chem. Phys.* **122**, 224322; 10.1063/1.1940588 (2005).
21. Foulkes, W. M. C., Mitas, L., Needs, R. J. & Rajagopal, G. Quantum Monte Carlo simulations of solids. *Rev. Mod. Phys.* **73**, 33; 10.1103/RevModPhys.73.33 (2001).
22. Lee, R. M., Conduit, G. J., Nemeč, N., Ríos, P.L. & Drummond, N. D. Strategies for improving the efficiency of quantum Monte Carlo calculations. *Phys. Rev. E* **83**, 066706; 10.1103/PhysRevE.83.066706 (2011).
23. Sumimoto, M., Kawashima, Y. Hori, K. & Fujimoto, H. Theoretical investigation of the molecular and electronic structures and excitation spectra of iron phthalocyanine and its derivatives, FePc and FePcL<sub>n</sub> (L=Py, CN<sup>-</sup> ; n=1,2). *Dalton Trans.* 5737–5746; 10.1039/B823309H (2009).
24. Inuzuka, K. Near Ultraviolet Absorption Spectra of Acrolein and Crotonaldehyde. *Bull. Chem. Soc. Jap.* **33**, 678–680; 10.1246/bcsj.33.678 (1960).
25. Blom, C. E., Grassi, G. & Bauder, A. Molecular Structure of s-cis- and s-trans-Acrolein Determined by Microwave Spectroscopy. *J. Am. Chem. Soc.* **106**, 7427–7431; 10.1021/ja00336a022 (1984).
26. Choe, Y.-K., Hashimoto, T., Nakano, H. & Hirao, K. Theoretical study of the electronic ground state of iron(II) porphine. *Chem. phys. Lett.* **295**, 380–388; 10.1016/S0009-2614(98)00986-5 (1998).